Engineering Structures 100 (2015) 293–307

Contents lists available at ScienceDirect

Engineering Structures

journal homepage: www.elsevier.com/locate/engstruct

# Block shear strength and design of coped beams with double bolt-line connections

Angus C.C. Lam [a], Cheng Fang [b,c,*], Michael C.H. Yam [d], Wei Wang [a], V.P. Iu [a]

[a] Department of Civil & Environmental Engineering, University of Macau, Macau, China
[b] Department of Structural Engineering, College of Civil Engineering, Tongji University, Shanghai 200092, China
[c] School of Civil Engineering and Geosciences, Newcastle University, Newcastle upon Tyne NE1 7RU, United Kingdom
[d] Department of Building & Real Estate, The Hong Kong Polytechnic University, Hung Hom, Kowloon, Hong Kong, China

ARTICLE INFO

*Article history:*
Received 13 November 2014
Revised 1 June 2015
Accepted 10 June 2015
Available online 24 June 2015

*Keywords:*
Block shear
Coped steel beams
Double bolt-line
Full-scale tests
Reliability analysis
Design

ABSTRACT

Available test data on block shear behaviour of coped beams with double bolt-line connections are quite limited, and earlier investigations found that the test block shear capacities could not be accurately predicted by existing design rules which deal with this failure mode in an inconsistent manner. To address this, a comprehensive investigation focusing on the block shear behaviour of coped beams with double bolt-line connections was reported in this paper. The research commenced with 17 full-scale tests considering the test parameters of web block aspect ratio, out-of-plane eccentricity, connection rotational stiffness, and bolt stagger. Two specimens were found to fail by local web buckling, and the remaining 15 specimens failed by block shear. Three typical block shear failure modes were observed at ultimate load, namely, whole block tear-out (WBT), tensile fracture (TF), and tensile fracture followed by whole block tear-out (TF–WBT). The influences of the considered test parameters on the failure mode and block shear capacity of the test specimens were thoroughly discussed. The test results were then compared with existing design rules to evaluate the consistency and accuracy of the major standards, and it was found that these standards led to inconsistent test-to-predicted ratios and tended to be conservative. Summarising all available test data, including the current tests and those previously conducted by other researchers, a reliability analysis was conducted to further examine the level of safety of the major standards. Design recommendations were finally proposed aiming to achieve reliable yet economical design approaches with consistent safety levels.



## 1. Introduction

It is very common in structural steel design to remove part of the flange of secondary beams in order to ensure the same elevation at member junctions. The beams with removed top flange (or both flanges if necessary) near the connection zone are called coped/notched beams. While the removal of part of the flange is one of the easiest solutions to provide the required clearance, the presence of the cope will inevitably reduce the strength of the beam in the coped region, and block shear is one of the most common failure modes for coped beams. This failure mode is typically featured by a block of material torn out from the coped beam web, and it can happen in either bolted or welded connections. For a bolted connection, where different numbers of bolt lines/rows (the definitions of which are shown in Fig. 1(a)) can be arranged to cater for various design requirements, block shear failure is often featured by a tensile fracture developed on the plane along the bottom bolt row (i.e. tension area) and a shear failure (either excessive yielding or complete fracture) developed over a critical bolt line (i.e. shear area). The typical block shear failure modes for the coped beams with single bolt-line and double bolt-line connections are shown in Fig. 1(a).

The block shear type of failure in coped beams was first observed during a test conducted by Birkemoe and Gilmor [1] initially aiming to examine the bolt bearing behaviour of coped beams. This unexpected failure mode raised great concerns among the researchers, and subsequent test programmes were launched by Yura et al. [2] and Ricles and Yura [3] to specifically investigate the block shear behaviour of coped beams. Elastic FE analysis was also performed to obtain the elastic stress distributions along the tensile and shear planes, based on which preliminary design rules were proposed which were later recommended by Kulak and Grondin [4]. Aalberg and Larsen [5] conducted eight tests on coped beams with single bolt-line connections, where both normal steel

* Corresponding author at: Department of Structural Engineering, College of Civil Engineering, Tongji University, Shanghai 200092, China. Tel.: +86 21 65983894.
*E-mail addresses:* chengfang@tongji.edu.cn, cheng.fang@ncl.ac.uk (C. Fang).

http://dx.doi.org/10.1016/j.engstruct.2015.06.019
0141-0296/

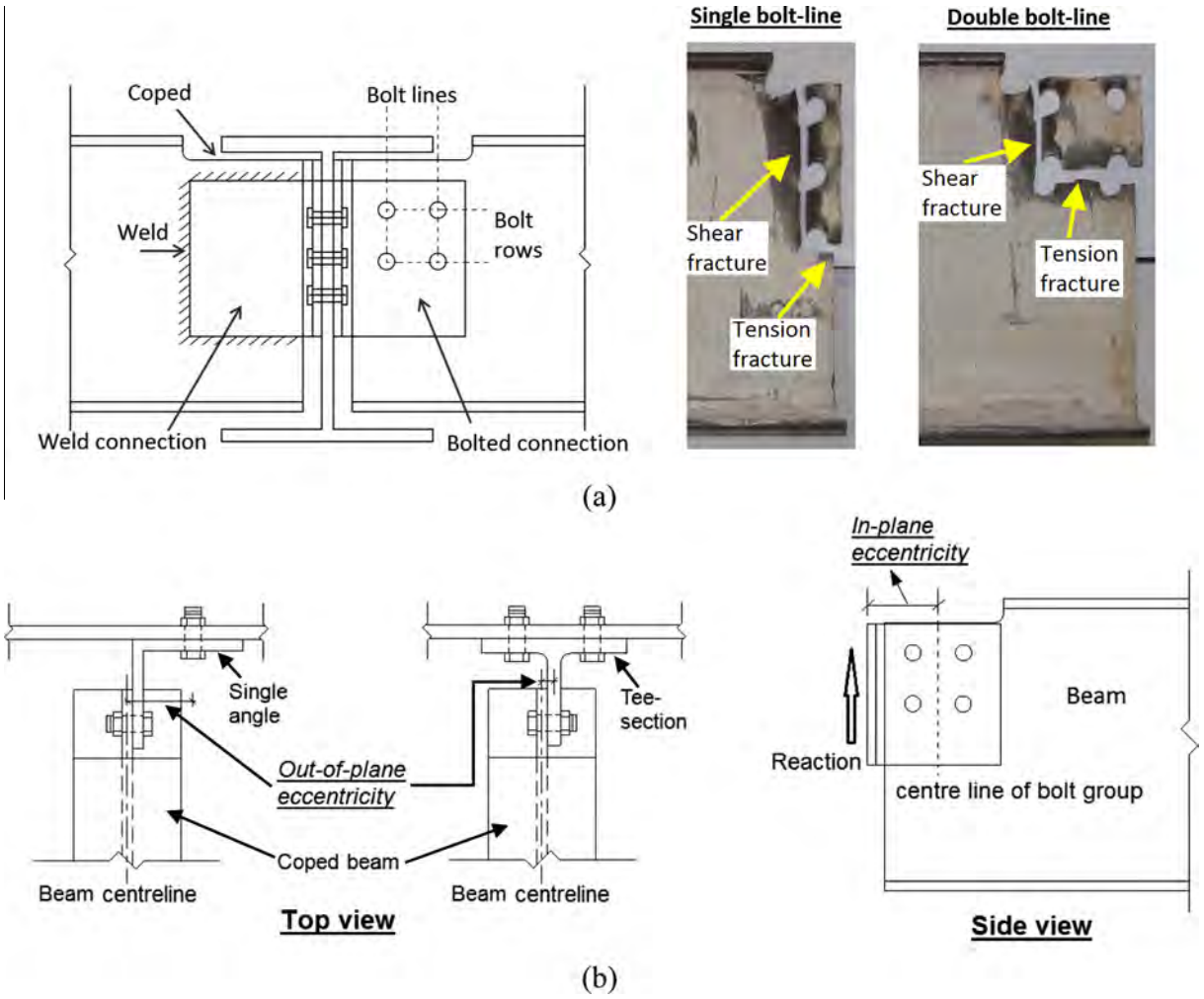


**Fig. 1.** Block shear failure of coped beams: (a) connections types and typical failure modes and (b) illustration of eccentricities.

and S700 high-strength steel (HSS) were considered. It was found that due to the relatively lower material ductility and tensile-to-yield strength ratio of HSS, the test-to-predicted ratios of the ultimate capacities for the normal strength steel specimens were generally higher than those for the HSS specimens. Franchuk et al. [6] expanded the test data pool by conducting 17 block shear tests on coped beams, where 14 specimens were single bolt-line connections and the remaining three were double bolt-line connections. The test parameters included beam end rotation, end and edge distances, and bolt layout. A reliability study was then performed by Franchuk et al. [7] based on the available test data, and it was found that the design models in major standards generally offer a reasonable level of safety for the case of single bolt-line connections; however, the block shear capacity of the coped beams with double bolt-line connections are often unsafely predicted with a relatively high level of variation. Topkaya [8] undertook a nonlinear FE analysis study on block shear behaviour of coped beams. A block shear model was developed which was found to have reasonable agreements with the FE results on the conservative side. More recently, the authors [9] conducted ten block shear tests on coped beams, including seven specimens with single bolt-line connections and three with double bolt-line connections. The focus was given to the effect of out-of-plane eccentricity due to the use of single-sided connections. The out-of-plane eccentricity was defined as the distance between the centre line of the beam web and the centroid of the reaction force, as illustrated in Fig. 1(b). No detrimental effect due to the out-of-plane eccentricity was found on the block shear capacity of the specimens with single bolt-line connections, but inconsistent results were observed for those with double bolt-line connections. It was also found that the current design rules can be overly conservative for the case of double bolt-line connections, which seemed to contradict the finding reported by Franchuk et al. [6,7]. But it should be noted that some standards considered in Franchuk et al. [6,7] were based on their earlier versions which were later updated. The major research efforts in the field of block shear has been summarised in a recent state-of-the-art investigation carried out by the authors [10].

It can be seen from the available literature that the block shear capacity of coped beams with double bolt-line connections is not well predicted by existing design models, and inconsistent findings have been reported by different researchers. Importantly, existing research emphasis was mainly given to the coped beams with single bolt-line connections, whereas insufficient test data are available for the case of double bolt-line connections. Compared with the former case, block shear of coped beams with double bolt-line connections can be a more complex issue. The main reason is that the use of double bolt-line leads to two segments along the tension area, which can lead to significant non-uniform stress distributions. The additional bolt line can induce an increased in-plane eccentricity at the beam end (the definition of in-plane eccentricity is shown in Fig. 1(b)), which further complicates the stress distribution and fractural behaviour of the tension area, especially when the connection is flexible. In fact, one of the most controversial aspects in the block shear design of coped beams

with double bolt-line connections is the determination of the utilisation/efficiency factor along the tension area, and the value can vary significantly in different design standards. This may explain the high level of inconsistency observed from the limited available test data. In order to provide more test evidence for the case of double bolt-line connections, a total of 17 full-scale tests, covering the variations of web block aspect ratio, out-of-plane eccentricity, connection rotational stiffness, and bolt stagger, are reported in this study. The test results are compared with existing design rules to evaluate the consistency and rationale behind the major standards, and this is followed by a reliability analysis to further examine their levels of safety. Design recommendations are finally proposed aiming to achieve reliable yet economical design approaches with consistent safety levels.

## 2. Experimental programme

### 2.1. Test specimens

A total of 17 specimens were tested in the experimental programme, where double bolt-line connections were employed for all the specimens. Nine UB406 × 140 × 46 test beams [11] of 3.4 m long were used to produce the desirable coped beam end details for the 17 tests. The measured dimensions for each beam are given in Table 1 and the relevant symbols are illustrated in Fig. 2. The main test parameters of the specimens were web block aspect ratio $b/a$ (hereafter named as 'aspect ratio'), out-of-plane eccentricity, connection rotational stiffness, and bolt stagger. The aspect ratio was varied by changing the end distance ($e_h$), top edge distance ($e_d$), horizontal bolt spacing ($g$), and vertical bolt spacing ($s$), as marked in Fig. 2. The out-of-eccentricity and connection rotational stiffness were varied by using different types of connections, i.e. double angle cleat connections, single angle cleat connections, and tee connections. Standard T178 × 203 × 30 and T210 × 267 × 61 sections [11] were employed for the T1 and T2 connections, respectively. For the angles, the nominal thickness ($t$) of A1 and A2 was 16 mm, but the length of leg ($h$) for the two angles was slightly different in order to accommodate the different $e_h$ and $g$ values at the beam end ($h$ = 200 mm for A1 and $h$ = 180 mm for A2). The value of $x$ (as marked in Fig. 2) was adjusted to ensure that the same gauge length (and therefore the same rotational stiffness) was considered for A1 and A2. The size of A3 (nominal $t$ = 10 mm, $h$ = 150 mm) was designed to be smaller than A1 and A2 in order to consider the effect of smaller connection rotational stiffness. Two other specimens using single A2 were also tested to consider the effects of large out-of-plane eccentricity. The measured values for the beam ends and connections are given in Table 2, which also shows the measured values of aspect ratio ($b/a$) and out-of-plane eccentricity.

For easy identification, each specimen was assigned with a specimen code according to the connection type and beam end bolt arrangement. For the specimens with double angle cleat or tee connections, the specimen code starts with the connection type, followed by the nominal values of bolt spacing $g$ and $s$. As the standard nominal value of $e_h$ and $e_d$ is 28 mm, any change of these is reflected in the end of the specimen code. For example, T1G75S75-$e_h$50 represents the specimen with a T1 type connection and both the nominal horizontal bolt spacing ($g$) and vertical bolt spacing ($s$) equal to 75 mm; the nominal end distance ($e_h$) is increased to 50 mm, while the top edge distance ($e_d$) is kept as 28 mm. For the single angle cleat connections, the specimen code starts with SA2 (angle A2 was used), and ends with the $x$ value which was different for the two specimens. For the two staggered bolt cases, the specimen code ends with ST1 and ST2, where the details of the staggered patterns are shown in Fig. 2. Grade S355 steel was used for the beams and connections. The coupon tests were conducted according to the ASTM specification [12]. The average values of Young's modulus, yield strength, tensile strength, and rupture strain obtained from the coupon tests are shown in Table 3. For the beam web and flange, the results shown in Table 3 were based on the average values of six coupons for each part, and for the other components, the average values of four coupons were given. Grade 12.9 M22 snug-tightened bolts were used for the connections except for the bolt line which connects the single angle cleat connection to the column face, where grade 12.9 M24 bolts were used instead.

### 2.2. Test setup, instrumentations, and test procedures

The test setup was designed to enable a statically determinate beam to be supported by a bolted connection at the coped end and a roller support at a distance of 2000 mm away from the coped end, as illustrated in Fig. 3. The loading position was located at a distance of 600 mm from the coped end, and a hydraulic jack with a maximum capacity of 1000 kN was used to apply the point load to the test beams. Load cells were used at both the loading position and the far end support to record the applied load $P$ and the reaction $R_1$, such that the reaction $R$ at the coped end can be easily calculated (i.e. $R = P - R_1$). Lateral bracings were provided to prevent lateral movements of the beam. Whitewash was applied on the test beam to show any yield pattern during the tests. It should be noted that this test setup could lead to slightly different deformation mode of the beam from that in a real structure if the beam is a component of a typical gravity floor framing system. However, due to the way that the test beam rotates, it was considered that the test case could lead to more significant stress concentration at the $e_h$ segment than the actual case. As the $e_h$ segment plays a critical role in determining the block shear capacity of coped beams, it is reasonable to believe that the test case is on the conservative side. Nevertheless, further studies may be necessary to more accurately consider this effect.

**Table 1**
Measured geometric properties of test beams (UB406 × 140 × 46).

| Beam No. | Specimen code | $B$ | $D$ | $T_w$ | $T_f$ | Beam No. | Specimen code | $B$ | $D$ | $T_w$ | $T_f$ |
|---|---|---|---|---|---|---|---|---|---|---|---|
| 01 | SA2G75S75-x90<br>A2G75S75-ST2 | 142.3 | 403.0 | 6.8 | 11.2 | 06 | T1G75S75-$e_h$50<br>T2G75S75-$e_h$50 | 142.5 | 403.0 | 6.8 | 11.1 |
| 02 | T1G75S75<br>T2G75S75 | 142.0 | 403.0 | 7.1 | 10.9 | 07 | A1G75S75-$e_h$50<br>A1G97S75 | 142.6 | 403.0 | 6.7 | 11.0 |
| 03 | T1G75S112.5<br>T1G75S75-$e_d$65.5 | 142.0 | 403.0 | 6.8 | 10.8 | 08 | A2G75S112.5<br>A2G75S75-$e_d$65.5 | 142.5 | 403.7 | 6.8 | 11.2 |
| 04 | T1G97S75<br>T2G97S75 | 142.0 | 403.0 | 7.0 | 10.8 | 09 | A2G75S75-ST1 | 142.0 | 403.0 | 7.0 | 10.7 |
| 05 | SA2G75S75-x120<br>A3G75S75 | 142.0 | 403.0 | 6.9 | 11.0 | | | | | | |

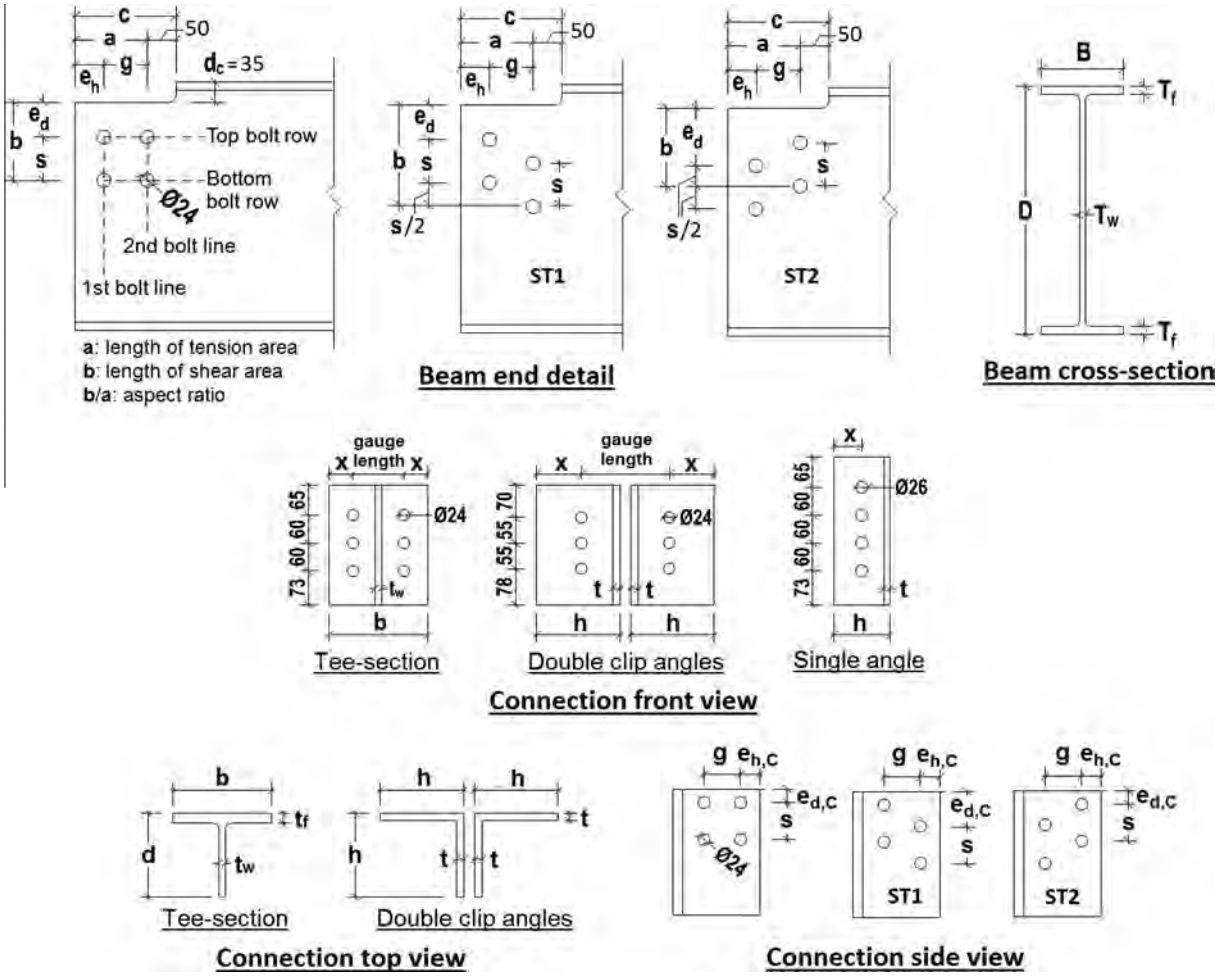


**Fig. 2.** Symbols and dimensions of beams and connections – unit in mm.

**Table 2**
Measured geometric properties of beam ends and connections.

| Specimen code | $g$ | $s$ | $e_h$ | $e_d$ | $b$ | $d$ | $t_w$ | $t_f$ | $h$ | $t$ | $x$ | $e_{h,c}$ | $e_{d,c}$ | $b/a$ | *Ecc.* |
|---|---|---|---|---|---|---|---|---|---|---|---|---|---|---|---|
| T1G75S75 | 75.4 | 75.2 | 30.5 | 27.7 | 178.0 | 192.5 | 8.0 | 12.6 | – | – | 32.7 | 39.3 | 29.2 | 0.97 | 7.6 |
| T1G75S112.5 | 75.3 | 112.8 | 28.6 | 27.9 | 178.0 | 192.8 | 7.8 | 12.8 | – | – | 35.8 | 39.7 | 29.4 | 1.35 | 7.3 |
| T1G97S75 | 97.3 | 74.7 | 29.5 | 28.4 | 178.8 | 192.8 | 7.9 | 12.6 | – | – | 35.4 | 39.4 | 28.7 | 0.81 | 7.5 |
| T1G75S75-$e_h$50 | 75.0 | 76.0 | 50.0 | 29.0 | 178.0 | 194.0 | 7.9 | 12.5 | – | – | 34.0 | 40.0 | 27.0 | 0.84 | 7.4 |
| T1G75S75-$e_d$65.5 | 74.5 | 74.4 | 27.5 | 64.9 | 177.8 | 193.5 | 7.9 | 12.9 | – | – | 35.4 | 38.9 | 66.0 | 1.37 | 7.4 |
| T2G75S75 | 74.6 | 74.2 | 32.0 | 28.1 | 210.2 | 200.0 | 12.7 | 21.4 | – | – | 56.2 | 39.3 | 28.9 | 0.96 | 9.9 |
| T2G97S75 | 96.5 | 75.5 | 26.7 | 27.9 | 210.0 | 202.8 | 12.7 | 21.5 | – | – | 52.7 | 41.1 | 27.7 | 0.84 | 9.9 |
| T2G75S75-$e_h$50 | 75.0 | 75.0 | 50.0 | 28.0 | 210.2 | 201.0 | 12.7 | 21.3 | – | – | 51.0 | 39.0 | 27.0 | 0.82 | 9.8 |
| A1G97S75 | 97.0 | 75.0 | 28.0 | 28.0 | – | – | – | – | 200.0 | 16.0 | 116.9 | 42.0 | 27.0 | 0.82 | 0 |
| A1G75S75-$e_h$50 | 75.0 | 75.0 | 50.0 | 28.0 | – | – | – | – | 200.0 | 16.0 | 116.1 | 42.0 | 27.0 | 0.82 | 0 |
| A2G75S112.5 | 75.0 | 113.0 | 28.0 | 28.0 | – | – | – | – | 180.0 | 16.0 | 96.0 | 42.0 | 27.0 | 1.37 | 0 |
| A2G75S75-$e_d$65.5 | 75.0 | 75.0 | 28.0 | 65.2 | – | – | – | – | 180.0 | 16.0 | 96.9 | 42.0 | 64.0 | 1.36 | 0 |
| SA2G75S75-x90 | 74.9 | 74.6 | 28.8 | 27.7 | – | – | – | – | 178.5 | 15.5 | 91.1 | 41.9 | 29.9 | 0.99 | 90.9 |
| SA2G75S75-x120 | 75.4 | 74.9 | 29.0 | 28.4 | – | – | – | – | 182.0 | 15.8 | 120.5 | 41.7 | 31.6 | 0.99 | 65.0 |
| A2G75S75-ST1 | 75.0 | 75.0 | 28.0 | 28.0 | | | | | 180.0 | 16.0 | 96.9 | 42.0 | 65.5 | 1.36 | 0 |
| A2G75S75-ST2 | 74.8 | 74.0 | 29.5 | 65.4 | – | – | – | – | 180.5 | 15.5 | 97.8 | 42.3 | 31.6 | 0.98 | 0 |
| A3G75S75 | 75.5 | 74.9 | 25.6 | 28.2 | – | – | – | – | 149.0 | 10.2 | 67.0 | 40.1 | 26.0 | 1.02 | 0 |

Note: $b/a$ = aspect ratio, *Ecc.* = out-of-plane eccentricity.

The vertical and horizontal displacements of the coped region were recorded by various linear variable differential transformers (LVDTs) as shown in Fig. 3. A series of longitudinal strain gauges and rosettes were mounted in the vicinity of the tension area and shear area. The strains at some other parts of the coped region were also monitored. Typical strain gauge locations for the cases of normal and staggered bolt arrangements are shown in Fig. 3. For the test procedure, the point load was incrementally applied using load control in the early loading stage, and slow stroke control was subsequently used in the inelastic stage in order to capture the nonlinear load–deflection behaviour. The test was terminated when either whole web block tear-out or rapid unloading occurred.

**Table 3**
Specimen material properties.

| Material | Young's modulus (MPa) | Static yield strength (MPa) | Static ultimate strength (MPa) | Rupture strain (%) |
|---|---|---|---|---|
| Beam web | 197,797 | 381.1 | 476.7 | 17.8 |
| Beam flange | 201,799 | 345.8 | 465.8 | 19.1 |
| Tee web (T1) | 198,988 | 412.2 | 514.0 | 16.3 |
| Tee web (T2) | 200,630 | 435.2 | 521.2 | 16.0 |
| Tee flange (T1) | 202,745 | 395.1 | 518.1 | 19.9 |
| Tee flange (T2) | 204,695 | 383.5 | 501.1 | 23.5 |
| Angle (A1&A2) | 195,075 | 418.5 | 513.3 | 18.4 |
| Angle (A3) | 189,923 | 377.0 | 521.2 | 16.3 |

As both ends of one test beam were designed as independent test specimens, after completing the test on one beam end, the beam was rotated and installed for the subsequent test at the other end.

## 3. Test results

### 3.1. General

Among the 17 tests conducted, 15 specimens failed by block shear, and the remaining two specimens failed by local web buckling. The typical block shear fractural patterns of the specimens are shown in Fig. 4. The ultimate reactions $R_u$ of the specimens ranged from 307.3 kN to 462.1 kN, depending on different connection details and bolt patterns. For the specimens failed by block shear, three typical failure modes were generally observed at ultimate load, namely, whole block tear-out (WBT), tensile fracture (TF), and tensile fracture followed by whole block tear-out (TF–WBT). The WBT failure mode was featured by a sudden fracture developed along both the tension and shear area (almost simultaneously), leading to the whole block torn from the coped region at ultimate load. The TF failure mode was featured by a complete fracture along the tension area combined with significant yielding along the shear area at ultimate load. For the TF–WBT failure mode, fracture occurred first along the $e_h$ segment of the tension area, but further loading can be sustained until the occurrence of the subsequent fracture along the remaining tension area and shear area, leading to whole block tear-out at ultimate load. For the two specimens with the staggered bolt arrangements, one failed by TF and the other one failed by TF–WBT. For both cases, tensile fracture was originated from the beam end and propagated beyond the first bolt line towards the second bolt line with an inclined propagation angle. The tensile fractural route exhibited a typical zigzag pattern. The shear failure mode for the specimens with the staggered bolt arrangements was similar to that for the other specimens. Some specimens with single-sided connections (i.e. with tee or single angle cleat connections) showed web twisting due to the presence of out-of-plane eccentricity, and the significance of web twisting seemed to be dependent on the lateral stiffness of the connection, as further discussed in Section 4. The photos of typical web twisting deformation of the coped web are shown in Fig. 4. The ultimate load $P_u$, ultimate reaction $R_u$, vertical displacement at ultimate load $\delta_u$ (i.e. the reading of LVDT6 at ultimate load), and failure mode of the specimens are summarised in Table 4.

### 3.2. Load–deflection response

The load–deflection responses of the test specimens are shown in Fig. 5, where the vertical displacements were based on the readings from LVDT6. It should be noted that the load–deflection response for specimen A2G75S75-ST2 is not shown in the figure as malfunction of the LVDT occurred during the test. Linear load–deflection responses were generally observed at the initial loading stage, which was then followed by nonlinear responses initiated at approximately 80% of the ultimate load. The minor difference of the initial stiffness (slope) among different specimens might be due to varied significance of bolt slippage. The different levels of rotational stiffness provided by various end connections might also attribute to the slight difference of the initial load–deflection stiffness. At the inelastic stage, the load–deflection response was related to the failure mode/sequence. For the specimens failed by WBT mode, e.g. T2G75S75, the load tended to drop abruptly after reaching the ultimate load. For the specimens failed by TF mode, e.g. A2G75S112.5, the ultimate load was achieved when complete tensile fracture occurred, and for some cases two adjacent peaks were shown, indicating first tensile fracture over $e_h$ and the propagated tensile fracture between the first and second bolt lines. After that, the sustained load level decreased, but some residual load carrying capacity was still maintained in the manner of shear yielding over the shear area. During this stage, the sustained load might regain slightly, which was quickly followed by a second drop of the load–deflection curve due to the entire fracture of the shear area. For those failed by TF–WBT mode at ultimate load, e.g. A1G97S75, two peaks were typically shown in the load–deflection curve. The first peak corresponded to the initial tensile fracture over $e_h$, while the second peak, where the ultimate load was reached, indicated a whole block tear-out. For specimens T1G75S75-$e_h$50 and T2G75S75-$e_h$50 which failed by local web buckling, the load started to decrease after the occurrence of local web buckling. The load–deflection curves were quite similar to those reported in the other studies on local web buckling of coped beams [13,14].

### 3.3. Strain gauge readings

A series of strain gauges were mounted in the vicinity of tension and shear areas to monitor the corresponding strain distributions, where the typical strain gauge readings are shown in Fig. 6. Non-uniform tensile strain distributions were observed over the measured area which was 30 mm below the bottom bolt row. The strain distributions became more nonlinear with the increasing of the applied load. In general, a high level of strain was developed close to the beam end, but the strain decreased evidently at the location immediately below the first bolt line. The strain level tended to increase again over the area between the first and second bolt lines, especially when the applied load was increased, but beyond the second bolt line, the strain dropped quickly, which implied that the last measured location of the strain gauge series along the tension area was outside the critical fractural zone. The tensile strain distribution also indicated that first tensile fracture was originated from the beam end over the $e_h$ segment, where the highest strain level was observed. This is in line with the test observations, especially for those failed by TF and TF–WBT. It should be noted that for specimen T2G97S75, the tensile strain near the beam end dropped significantly at the applied load of

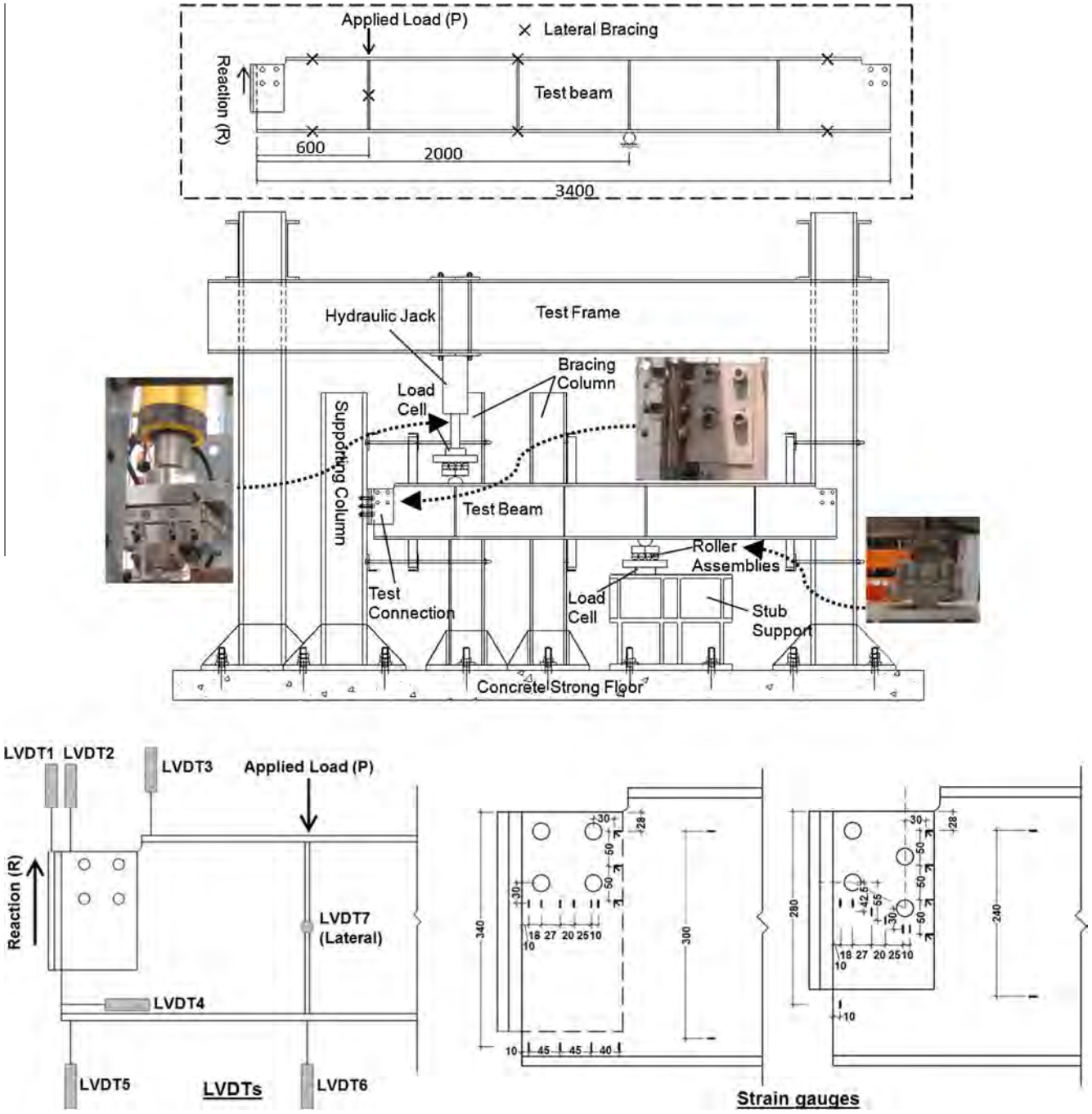


**Fig. 3.** Test setup and instrumentations.

590 kN. This was due to a complete fracture over $e_h$ at that load level. This also explains the suddenly increased strain level between the first and second bolt lines, which was due to the stress redistribution after initial fracture. Typical shear strain distributions obtained from the rosettes near the shear area are also shown in Fig. 6. At initial loading stages, e.g. $P = 100$ kN, a relatively low level of shear strain variations was observed. With the increase of the load, the shear strain distribution became more non-uniform, and the high shear zone seemed to be dependent on the bolt pattern. In general, larger shear strain could be exhibited near the bolt areas, and this is in line with the shear strain distribution reported by Ricles and Yura [3] through elastic FE analysis.

## 4. Discussion of test results

### 4.1. Factors influencing failure mode

Compared with the case of single bolt-line connections, the failure mode of the double bolt-line specimens could be more complex, and was largely dependent on the bolt arrangement. In general, WBT (whole block tear-out) at ultimate load could be more likely to occur in the specimens with a lower aspect ratio (i.e. a lower shear/tension area ratio). This is because that excessive shear yielding had already been developed over the relatively small shear area prior to tensile fracture. When tensile fracture was about to occur, the load resisting demand was largely

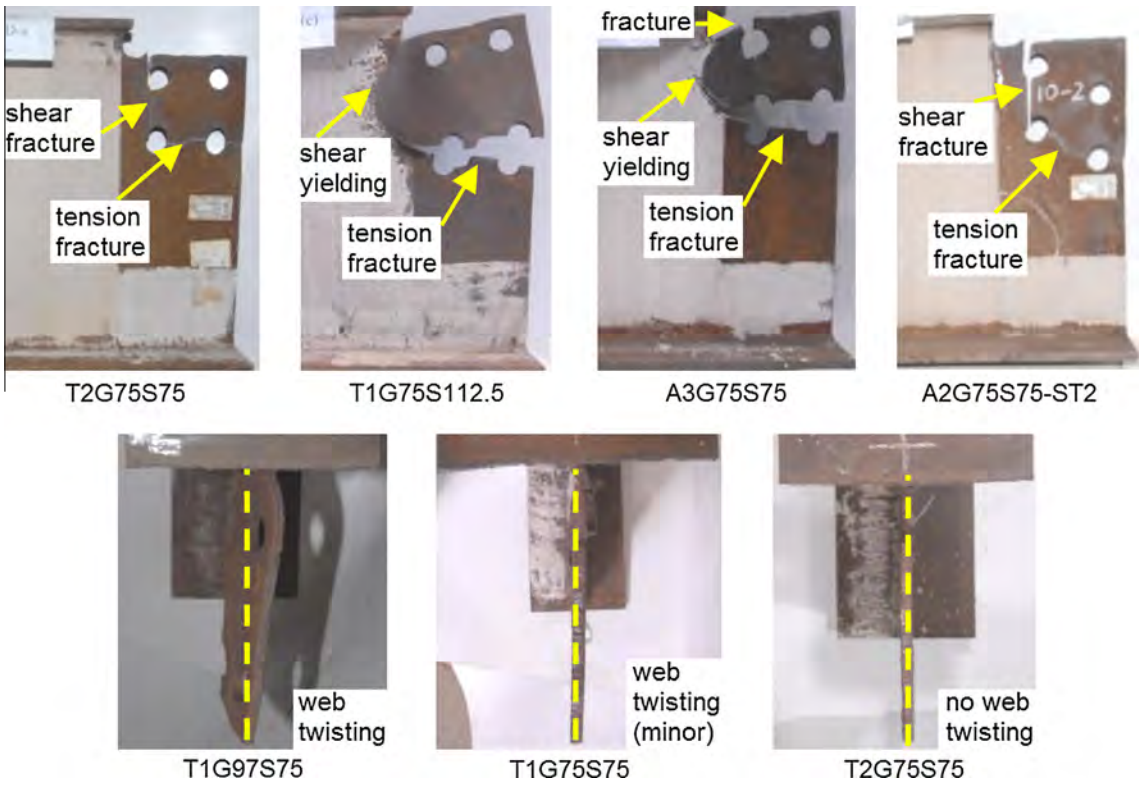


**Fig. 4.** Typical block shear failure modes of specimens.

accommodated by the shear area, and the very limited reserve of the load carrying capacity offered by the shear area was quickly exhausted, leading to the WBT failure mode at ultimate load. On the other hand, when the shear area was relatively large, the occurrence of tensile fracture led to no immediate fracture of the shear area, and thus the typical failure mode at ultimate load was exhibited by tensile fracture with significant shear yielding (i.e. TF mode). It was also found that the distance between the beam end and the first bolt line, i.e. the length of $e_h$, could evidently influence the failure mode. No block shear failure was observed in specimens T1G75S75-$e_h$50 and T2G75S75-$e_h$50, where local web buckling occurred instead. It was believed that the occurrence of LWB was due to two major reasons: firstly, the increase of the length of $e_h$, which caused an increase of the cope length $c$, could make the specimens more susceptible to LWB. This is because that local web buckling is mainly induced due to the compressive force developed at the top edge of the coped region when the beam is under bending, and therefore a longer coped length can decrease the local buckling resistance; and secondly, the increase of the length of $e_h$, which could evidently increase the block shear capacity (as can be confirmed in Table 4), postponed the occurrence of block shear failure, and thus LWB happened first. Moreover, it was of interest to observe that the TF–WBT failure mode tended to occur in the cases of $e_h$ = 28 mm with a relatively large $g$ value (i.e. $g$ = 97 mm). TF–WBT was also found in the case of ST2 staggered bolt pattern. The reason is that the relatively small length of $e_h$ could cause early fracture between the beam end and the first bolt row, but due to the increased length of $g$ (or because of the introduction of bolt stagger between the first and second bolt rows), the initial tensile fracture did not immediately propagate beyond the first bolt line. Therefore, WBT finally occurred after the initial fracture over the length of $e_h$, and the ultimate load was governed by TF–WBT.

Furthermore, the failure mode/sequence could also be affected by the connection type. The various rotational stiffness provided by the different connection types seemed to be one of the most important factors affecting the failure mode. In general, a more flexible connection could more likely cause the TF failure mode. The main reason is that, a low connection rotational rigidity caused more significant in-plane rotation of the 'block', which led to a more non-uniform stress distribution over the tension area with a higher stress level concentrated near the beam end. A similar phenomenon was found in the block shear tests of coped beams with welded connections [15]. The influence of connection rotational rigidity can also be confirmed via the strain distributions previously shown in Fig. 6. As can be seen in the top-left hand of Fig. 6, under the applied load of 100 kN, the strain gauge reading closest to the beam end for specimen A3G75S75 was significantly higher than those for its T1 and T2 counterparts. This implies that tensile fracture tended to occur earlier for specimen A3G75S75, at which point the shear area still had certain residual resistance to prevent immediate shear fracture. Therefore, specimen A3G75S75 failed by TF. A similar trend can be found through comparing specimen T1G97S75 with T2G97S75, where the former failed by TF and the latter failed by TF–WBT. Again, the main reason is that the T1 connection was more rotationally flexible than the T2 connection.

In addition, the significance of web twisting at failure was closely influenced by the connection types. For all the specimens with double angle cleat connections (i.e. no out-of-plane eccentricity), no web twisting was observed at failure. For the specimens with single-sided connections, different levels of web twisting were observed, which was largely dependent on the out-of-plane stiffness provided by the connections. The out-of-plane connection stiffness was majorly determined by the thickness of the longitudinal connection component (i.e. the angle leg attaching to the coped beam web or the tee stem). For the case of single-sided tee connections, more evident web twisting was observed for the specimens with T1 connections than those with T2 connections, because that the T2 connections

**Table 4**
Test results and design predictions.

| Researchers | Specimen code | Ultimate load $P_u$ (kN) | Ultimate reaction $R_u$ (kN) | Deflection $\delta_u$ (mm) | Failure mode at ultimate load | Web twisting | Test-to-predicted ratio | | | | | Aspect ratio $b/a$ |
|---|---|---|---|---|---|---|---|---|---|---|---|---|
| | | | | | | | AISC-LRFD | CSA-S16-09 | Eurocode 3 | AIJ | Ref [8] | |
| Current study | T1G75S75 | 515.5 | 374.1 | 11.5 | WBT | Yes (minor) | 1.47 | 1.44 | 1.68 | 1.17 | 1.14 | 0.97 |
| | T1G75S112.5 | 493.7 | 363.4 | 14.6 | TF | Yes | 1.16 | 1.16 | 1.36 | 0.98 | 1.01 | 1.35 |
| | T1G97S75 | 532.4 | 383.6 | 15.8 | TF | Yes | 1.34 | 1.39 | 1.51 | 1.03 | 1.01 | 0.81 |
| | T1G75S75-$e_h$50 | 525.3[a] | 382.8[a] | 16.9 | LWB | Yes | – | – | – | – | – | 0.84 |
| | T1G75S75-$e_d$65.5 | 548.8 | 396.9 | 15.0 | TF | Yes | 1.29 | 1.29 | 1.52 | 1.09 | 1.13 | 1.37 |
| | T2G75S75 | 597.9 | 432.7 | 9.7 | WBT | No | 1.70 | 1.67 | 1.94 | 1.35 | 1.31 | 0.96 |
| | T2G97S75 | 601.2 | 439.1 | 13.6 | TF–WBT | No | 1.57 | 1.61 | 1.76 | 1.21 | 1.19 | 0.84 |
| | T2G75S75-$e_h$50 | 610.6[a] | 452.6[a] | 15.5 | LWB | Yes | – | – | – | – | – | 0.82 |
| | A1G97S75 | 571.6 | 420.7 | 20.9 | TF–WBT | No | 1.56 | 1.60 | 1.75 | 1.20 | 1.17 | 0.82 |
| | A1G75S75-$e_h$50 | 634.8 | 462.1 | 17.3 | WBT | No | 1.71 | 1.76 | 1.92 | 1.32 | 1.29 | 0.82 |
| | A2G75S112.5 | 534.6 | 387.5 | 13.8 | TF | No | 1.24 | 1.24 | 1.46 | 1.05 | 1.09 | 1.37 |
| | A2G75S75-$e_d$65.5 | 551.2 | 399.1 | 11.3 | TF | No | 1.28 | 1.29 | 1.51 | 1.08 | 1.12 | 1.36 |
| | SA2G75S75-x90 | 470.0 | 342.5 | 14.8 | TF | Yes (minor) | 1.43 | 1.40 | 1.64 | 1.14 | 1.11 | 0.99 |
| | SA2G75S75-x120 | 602.6 | 441.1 | 13.8 | TF–WBT | No | 1.80 | 1.76 | 2.05 | 1.43 | 1.40 | 0.99 |
| | A2G75S75-ST1 | 581.0 | 422.5 | 14.0 | TF | No | 1.29 | 1.31 | 1.51 | 1.08 | 1.12 | 1.36 |
| | A2G75S75-ST2 | 540.1 | 386.5 | 7.9[b] | TF–WBT | No | 1.55 | 1.54 | 1.77 | 1.23 | 1.20 | 0.98 |
| | A3G75S75 | 430.5 | 307.3 | 11.3 | TF | No | 1.28 | 1.24 | 1.47 | 1.03 | 1.00 | 1.02 |
| | | | | | | Mean= | **1.45** | **1.45** | **1.66** | **1.16** | **1.15** | |
| | | | | | | CoV= | **13.5%** | **13.6%** | **12.3%** | **11.3%** | **9.8%** | |
| Yura et al. [2] | 18-10 | N/G | 494.0 | 7.1[b] | TF | No | 0.94 | 0.88 | 1.08 | 0.80 | 0.97 | 2.00 |
| | 18-11 | N/G | 449.5 | 3.2[b] | TF | No | 0.75 | 0.74 | 0.84 | 0.59 | 0.74 | 1.45 |
| | 18-12 | N/G | 676.4 | 16.3[b] | TF | LWB | 1.16 | 1.14 | 1.31 | 0.92 | 1.16 | 1.60 |
| Ricles and Yura [3] | 18-16 | N/G | 494.0 | 2.0[c] | TF | N/G | 1.00 | 0.93 | 1.15 | 0.84 | 1.03 | 2.00 |
| | 18-17 | N/G | 583.0 | 2.3[c] | TF | N/G | 1.06 | 1.03 | 1.20 | 0.84 | 1.06 | 1.60 |
| | 18-18 | N/G | 449.5 | 1.6[c] | TF | N/G | 1.00 | 0.95 | 1.26 | 0.88 | 1.02 | 1.75 |
| | 18-19 | N/G | 596.3 | 2.2[c] | TF | N/G | 1.09 | 1.06 | 1.31 | 0.92 | 1.09 | 1.60 |
| Franchuk et al. [6] | C2 | N/G | 537.0 | 4.0[c] | TF | No | 1.13 | 1.08 | 1.40 | 1.06 | 1.15 | 2.29 |
| | J1 | N/G | 667.0 | 3.2[c] | WBT | No | 1.37 | 1.32 | 1.70 | 1.29 | 1.38 | 2.29 |
| | J2 | N/G | 338.0 | 5.1[c] | WBT | No | 1.24 | 1.29 | 1.48 | 1.04 | 1.08 | 1.00 |
| Fang et al. [9] | A2-2-2-a | 529.7 | 384.0 | 10.7 | TF | No | 1.66 | 1.61 | 1.88 | 1.31 | 1.26 | 1.00 |
| | T1-2-2-a | 522.1 | 379.7 | 11.2 | TF | Yes | 1.63 | 1.58 | 1.85 | 1.29 | 1.24 | 1.00 |
| | T2-2-2-a | 455.4 | 329.0 | 7.5 | TF | Yes (minor) | 1.49 | 1.45 | 1.71 | 1.20 | 1.17 | 1.00 |
| | | | | | | All data Mean= | **1.33** | **1.31** | **1.54** | **1.08** | **1.13** | |
| | | | | | | All data CoV= | **19.8%** | **20.7%** | **18.7%** | **18.0%** | **11.9%** | |

Note: WBT = whole block tear-out, TF = tension fracture, TF–WBT = tension fracture over $e_h$ followed by whole block tear-out, LWB = local web buckling, N/G = not directly given in the literature, Bold: Mean and CoV of data.
[a] Ultimate load reached due to local web buckling.
[b] Connection deflection, equivalent to the reading of LVDT5.
[c] Net connection deflection, equivalent to the reading of LVDT5 minus LVDT2.

were more laterally rigid than the T1 connections. For the two specimens with single angle connections, minor web twisting was observed for specimen SA2G75S75-x90, while specimen SA2G75S75-x120 showed no obvious web twisting. The insignificant web twisting for both cases can be due to the fact that the thickness of the leg of A2 was relatively large ($t$ = 16 mm), and thus A2 was relatively rigid in the lateral direction. The more obvious web twisting for specimen SA2G75S75-x90 could be due to its larger out-of-plane eccentricity compared with that of specimen SA2G75S75-x120.

### 4.2. Influence of aspect ratio

The above discussions focused on the influential factors on the failure mode, while these factors also concurrently affected the block shear capacity. In the following discussions, the ultimate reaction $R_u$ is used to represent the block shear capacities of the specimens. The influence of aspect ratio can be evaluated through comparing the block shear capacities of the specimens with different bolt arrangements but with the same connection type. It was observed that increasing the aspect ratio by increasing the shear

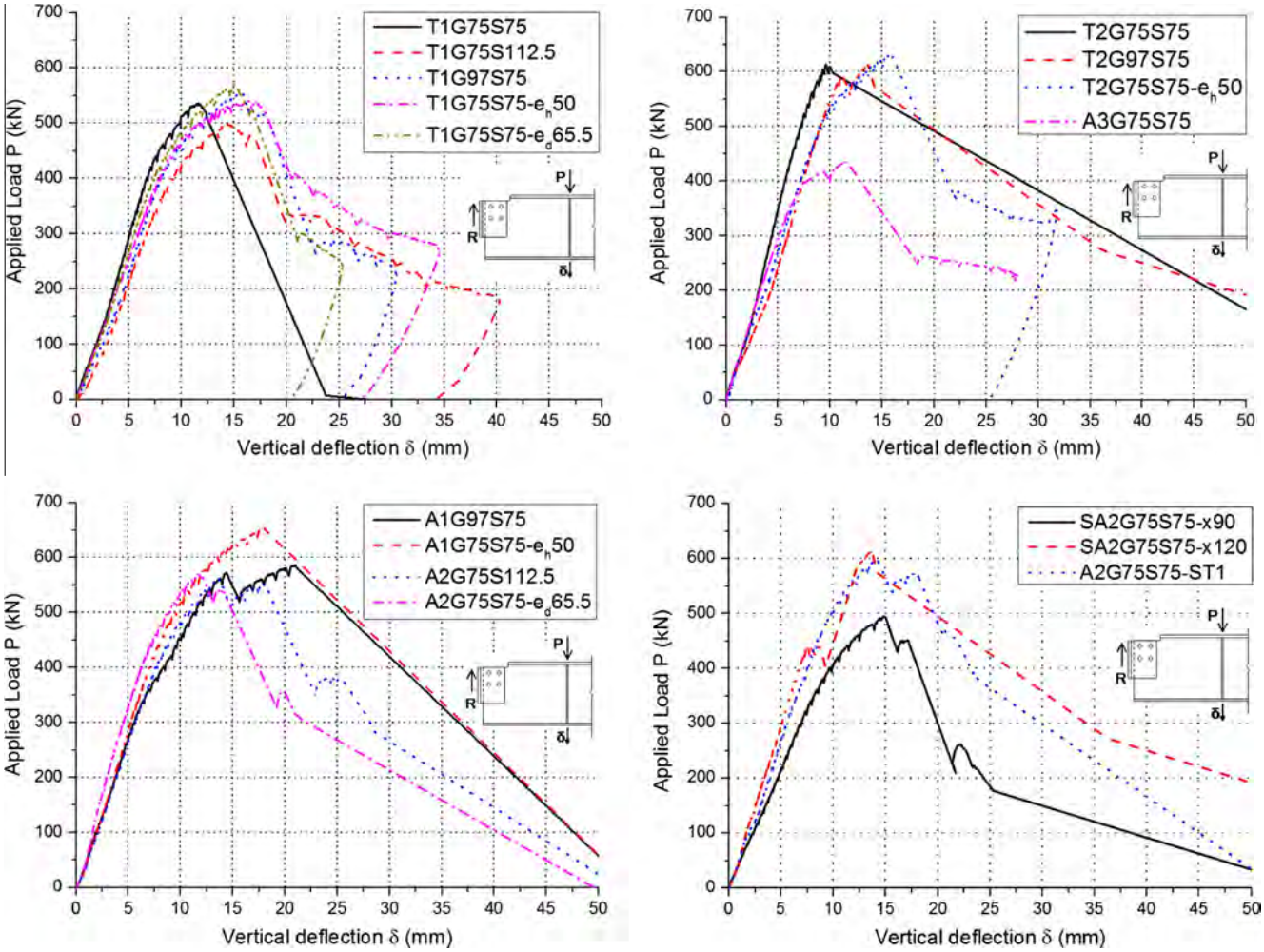


**Fig. 5.** Load–deflection responses of specimens.

area (while keeping the tension area unchanged) could increase the block shear capacity, but the beneficial influence was limited. As can be seen from Table 4 for T1 series, the ultimate reaction of specimen T1G75S75-$e_d$65.5 was only 6.0% higher than that of specimen T1G75S75, noting that the shear area for the former was 36.4% larger than that for the latter. It was also found that the ultimate reaction of specimen T1G75S112.5 was even 2.9% lower than that of T1G75S75, although the shear area for the former was larger. The above comparisons suggested that increasing the shear area has limited or no benefit for block shear capacity of coped beams with double bolt-line connections.

Increasing the tension area could also increase the block shear capacity, and it seemed that increasing $e_h$ could be more effective than increasing $g$. For T1 series, the ultimate reactions of specimens T1G97S75 and T1G75S75-$e_h$50 were 2.5% and 2.3% higher than that of T1G75S75, but it should be noted that the actual block shear capacity of T1G75S75-$e_h$50 could be evidently higher than the measured value because local web buckling occurred first. For T2 series, the ultimate reactions of specimens T2G97S75 and T2G75S75-$e_h$50 were 1.5% and 4.6% higher than that of T2G75S75, and again, a potentially higher block shear capacity is expected for T2G75S75-$e_h$50 as it failed by local web buckling. For the A1/A2 series, although no direction comparison could be made as there was no comparison set involving a pure change of the tension area, the ultimate reaction of specimen A1G75S75-$e_h$50 was evidently higher than those of the other A1/A2 specimens. This also indicates that increasing $e_h$ is effective in increasing the block shear capacity. The main reason for the effectiveness of increasing $e_h$ is that, as the initial tensile fracture always started from the $e_h$ segment, it is reasonable to believe that increasing the tensile capacity of the $e_h$ segment could benefit the block shear capacity. Among possible strategies, increasing the length of the $e_h$ segment is a convenient way to increase its tensile capacity because this could effectively postpone the initial tensile fracture via decreasing the tensile stress (due to increased length/area). In addition, the postponement of tensile fracture could allow more local deformation of the 'block' developed prior to tensile fracture, and as a result this could also allow the shear area to resist a higher shear load prior to tensile fracture, which might further contribute to the increase of the ultimate reaction.

### 4.3. Influence of connection rotational stiffness

An earlier study conducted by Yam et al. [15] showed that the rotational stiffness of the connection could have a significant effect on the block shear capacity of coped beams with welded connections, and this phenomenon was also found in this study. For the case of T series connections, where connection T2 was more rotationally rigid than connection T1 due to the larger flange thickness of the former, the specimens with T2 connections generally had higher ultimate reactions than those with T1 connections. For example, the ultimate reactions of specimens T2G75S75 and T2G97S75 were 15.7% and 14.5% higher than those of T1G75S75 and T1G97S75, respectively. The ultimate reaction of specimen

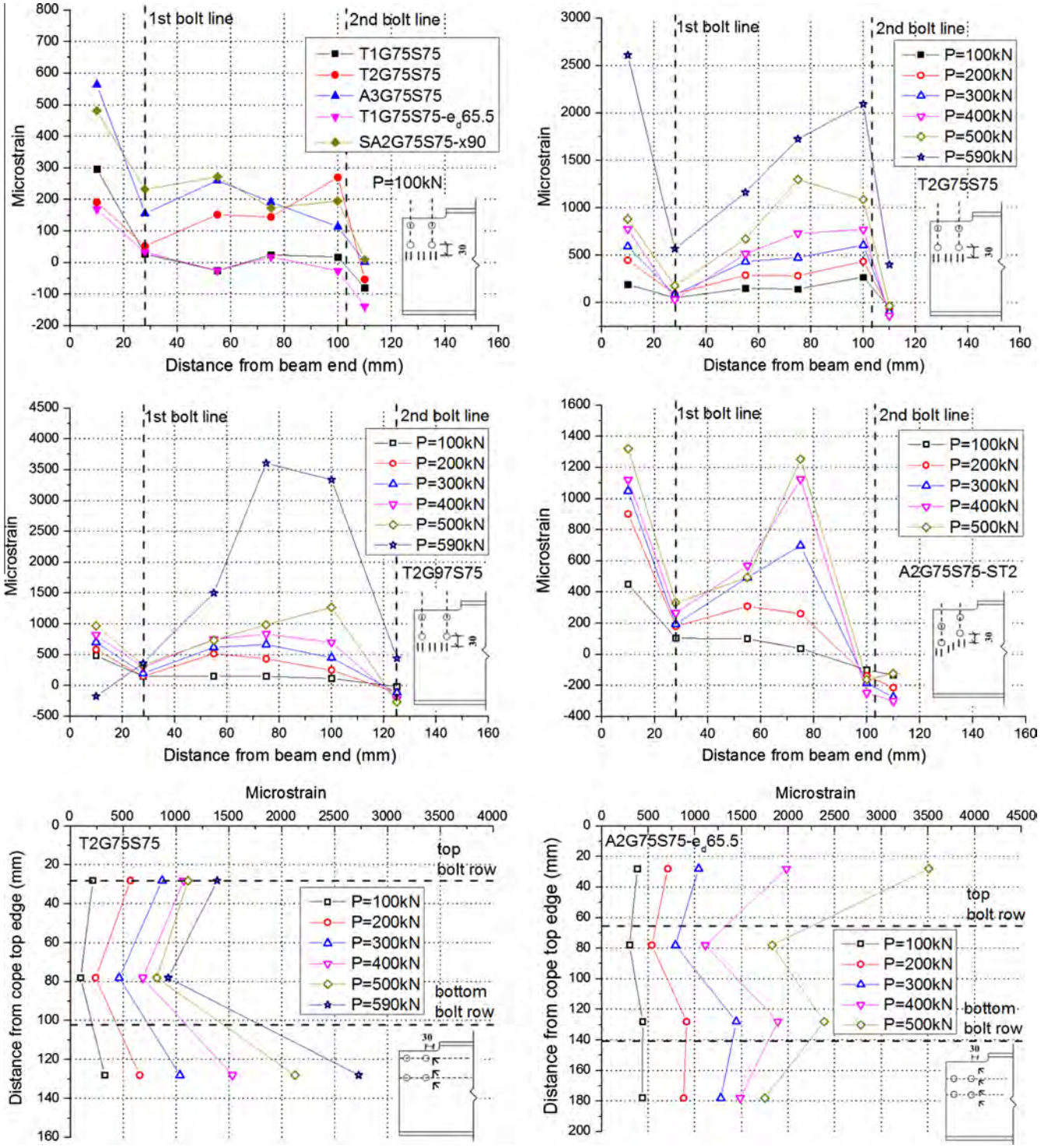


**Fig. 6.** Typical strain gauge readings of specimens.

T2G75S75-$e_h$50 was also higher than that of T1G75S75-$e_h$50 (increased by 18%), but it should be noted that both specimens failed by local web buckling. For specimen A3G75S75, where connection A3 exhibited the lowest rotational stiffness among all connections, the ultimate reaction of A3G75S75 was 17.9% and 29.0% lower than its T1 and T2 counterparts, respectively. As discussed previously in Section 4.1, the 'block' was more easily to be torn out when subjected to a higher level of in-plane rotation. This is due to the fact that a lower connection rotational stiffness could cause more non-uniform stress distributions over the tension area, and hence initiated early tensile fracture near the beam end where a higher stress level was concentrated.

### 4.4. Influence of out-of-plane eccentricity

A total of ten specimens with single-sided connections were tested in this study, where tee connections were employed for eight specimens, and single angle cleat connections were used for the remaining two. The main focus was to investigate the effect of the web twisting caused by out-of-plane eccentricity on the

block shear capacity of coped beams with double bolt-line connections. To examine this, the ultimate reactions of the T1 series specimens were compared with those of the A1/A2 series specimens, where obvious web twisting was found for all the T1 specimens while no web twisting was found in any A1/A2 specimen. Therefore, the following comparison group could be considered: (1) T1G75S112.5 and A2G75S112.5, (2) T1G97S75 and A1G97S75, and (3) T1G75S75-$e_d$65.5 and A2G75S75-$e_d$65.5, where the same bolt arrangement (but different out-of-plane eccentricities) was considered for each comparison set. For the three comparison groups, the T-to-A (tee-to-double angle) ultimate reaction ratios were 0.94, 0.91, and 1.00, respectively. This indicates that the ultimate reactions of the specimens with T1 connections tended to be slightly lower than those with A1/A2 connections. However, as discussed previously, the connection in-plane rotational stiffness also played an important role in determining the ultimate reaction, but it is difficult to directly compare the rotational stiffness of the two connection types since the flange thickness of T1 was less than that of A1/A2, however, the gauge length of T1 was also smaller. Therefore, simple FE models using ABAQUS [16] were established to assess the initial rotational stiffness of the connections, as shown in Fig. 7. The FE model was a cantilever system which was comprised of the considered connection that was fixed to an idealised rigid beam. The actual material properties of the connections obtained from the coupon tests were incorporated into the model. A static load was applied at the free end of the cantilever beam such that the moment–rotation response can be obtained. The FE modelling strategy was similar to that considered in another study conducted by the authors, as detailed in Fang et al. [9]. According to the FE analysis, the initial elastic rotational stiffness of connection T1 was 9300.2 kN m/rad, and that of connection A1/A2 was 10064.6 kN m/rad, i.e. connection T1 was less rotationally stiff than connection A1/A2. Therefore, the lower ultimate reactions of the T1 specimens compared with those of A1/A2 specimens might also be partially due to the lower rotational stiffness of connection T1.

For the two specimens with single-sided angle cleat connections, i.e. SA2G75S75-x90 and SA2G75S75-x120, the out-of-plane eccentricities were 90.9 mm and 65.0 mm, respectively. The ultimate reaction of SA2G75S75-x90 was 22.3% lower than that of SA2G75S75-x120. Again, the difference may be due to the combined effects of out-of-plane eccentricity and connection in-plane rotational stiffness, noting that the case of $x$ = 120 mm led to higher connection rotational stiffness than the case of $x$ = 90 mm. As both specimens showed insignificant web twisting, the effect of connection rotational stiffness might play a more critical role than the out-of-plane eccentricity for this comparison group.

In fact, a preliminary FE investigation focusing on the effect of out-of-plane eccentricity has been carried out by the authors [9]. It showed that for single bolt-line connections, the presence of out-of-plane eccentricity had no detrimental effect on the block shear capacity due to the possible beneficial effect of increased friction. For double bolt-line connections, the block shear capacity could be slightly decreased due to the out-of-plane eccentricity only when a very low connection stiffness was considered. Summarising the previously obtained FE results and the current test results, it can be preliminarily concluded that out-of-plane eccentricity may have detrimental effect on the block shear capacity for the case of double bolt-line connections, but the influence should be marginal. A comprehensive parametric study may be needed to further evaluate this detrimental effect accurately, but this is beyond the scope of this paper and hence will be discussed in a separate research paper.

### 4.5. Influence of bolt stagger

A staggered bolt arrangement can be associated with two main effects compared with the non-staggered case: (1) an effective length of $s_p^2/4g$ [17] may be added to the net tension area, i.e. $s_p^2/4g$ = 4.7 mm in this case, and (2) the shear area can be changed due to the vertical movement of the second bolt line. It should be noted that the $s_p^2/4g$ rule, where $s_p$ is the pitch ($s_p = s/2$ for the current specimens, where $s$ is given in Fig. 2) and $g$ is the gauge, has been widely used to calculate the effective net section of the zigzag path due to bolt stagger. For specimen A2G75S75-ST1, the second bolt line was moved downwards by 37.5 mm, and therefore the shear area was now the same as that for specimens A2G75S112.5 and A2G75S75-$e_d$65.5. It was found that the ultimate reaction of A2G75S75-ST1 was 9.0% and 5.9% higher than that of A2G75S112.5 and A2G75S75-$e_d$65.5, respectively, which could be due to the additional effective tension area according to the

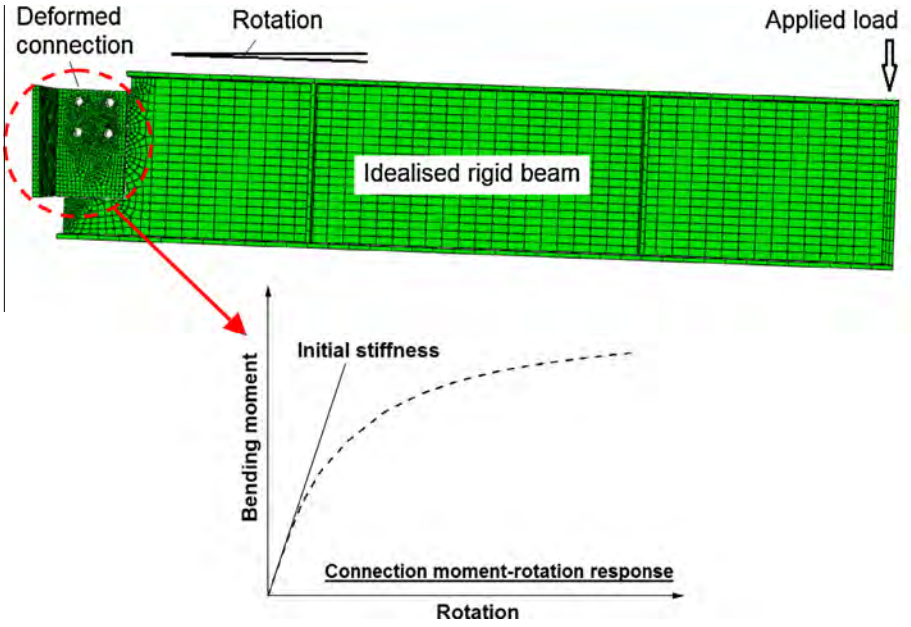


**Fig. 7.** FE models for rotational stiffness of connections.

$s_p^2/4g$ rule. The influence of bolt stagger may be approximately evaluated by considering a very basic block shear model which sums up the fracture resistance over the net tension area and yield resistance over the gross shear area, noting that more advanced models are available in major standards as will be discussed later. Using this basic model and considering the $s_p^2/4g$ rule, the block shear capacity of specimen A2G75S75-ST1 should be 3.5% higher than that of A2G75S112.5 or A2G75S75-$e_d$65.5. If an utilisation factor of 0.5 was applied on the tension area of the basic model, the increasing rate was only 2.3%. As the increasing rates based on the basic models were lower than the actual increasing rates (9.0% and 5.9%), it was suggested that purely using the $s_p^2/4g$ rule to approximate the effective tension area for the case of staggered bolt arrangement could be conservative, i.e. underestimated the increase of block shear capacity. For specimen A2G75S75-ST2, the first bolt line was moved downwards by 37.5 mm; therefore, an effective length of $s_p^2/4g$ was added to the tension area, but no change was made on the shear area. The actual ultimate reaction of A2G75S75-ST2 was found to be 8.1% lower than that of A1G97S75. Using the basic model discussed above and considering the $s_p^2/4g$ rule, the calculated block shear capacity of A2G75S75-ST2 should be 12.5% lower than that of A1G97S75. When an utilisation factor of 0.5 was considered for the basic model, the decreasing rate was 9.3%. This again implied that using the $s_p^2/4g$ rule for calculating the effective tension area could be safe and conservative.

Generally speaking, staggered bolt arrangements had minor and predictable influence on the block shear capacity of coped beams. The observed fracture pattern and the comparisons of ultimate reactions suggested that the $s_p^2/4g$ rule may be used to obtain the effective tension area for staggered bolt arrangements, and the way to determine the shear area can be the same as that for the case of non-staggered bolt arrangements. Through the relevant comparisons of the specimens with various bolt arrangements, it was preliminary concluded that simply calculating the effective tension area using the $s_p^2/4g$ rule for the case of staggered bolt arrangements can be safe (i.e. on the conservative side). Finally, it is worth mentioning that Epstein and Chamarajanagar [18] have studied the block shear performance of tension angles with staggered bolted connections. In that study, it was confirmed that bolt stagger pattern can influence the block shear capacity, but some negative effects (i.e. caused decreases of the block shear capacity) were observed for some specimens and FE models. However, the negative effects induced from bolt stagger were not observed in the current study, where both bolt stagger patterns were shown to benefit the block shear capacity of the coped beams. As the block shear performances of tension angles and coped beams could be different due to different connecting methods, loading directions, and boundary conditions, the outcome from the research on tension angles may not be directly applicable to the case of coped beams. Nevertheless, the result from Epstein and Chamarajanagar [18] warns that further studies may be required to ensure that the presence of bolt stagger causes no decrease of block shear capacity for coped beams, and thus more numerical and experimental investigations may be required on this front.

## 5. Comparisons against design standards

### 5.1. Existing design rules

Design equations for block shear are available in major standards, such as American Standard AISC-LRFD [19], Canadian Standard CSA-S16-09 [20], Eurocode 3 [21], and Japanese standard AIJ [22]. However, inconsistent design models are generally provided by these design standards, where the various design models are summarised in Table 5. AISC-LRFD assumes that the overall block shear capacity is the sum of the facture resistance over the net tension area and the resistance offered by the shear area. The resistance of shear area should be based on gross yielding or net rupture, whichever gives the less resistance. The efficiency/utilisation level of the tension area is considered by adding an $U_{bs}$ factor on the tensile fracture resistance, where $U_{bs}$ = 1.0 for the cases of single bolt line or welded connections, and $U_{bs}$ = 0.5 for the cases of double or multiple bolt lines. CSA-S16-09 adopts the same assumption to consider the resistance of tension area, i.e. fracture of the net tension area, but the use of utilisation factor $U_t$ is different, i.e. $U_t$ = 0.9 for coped beams with single bolt-line connections, and $U_t$ = 0.3 for those with double bolt-line connections. The shear resistance is the gross shear area multiplied by the average value of the yield and ultimate shear strengths. Eurocode 3 assumes that the block shear capacity is governed by tensile fracture of the net tension area and shear yielding on the net shear area. A consistent utilisation factor of 0.5 is applied to the resistance of tension area, regardless of the number of bolt lines. Finally, AIJ considers two possible failure modes, which are (1) fracture over the net tension area in combination with yielding over the net shear area, and (2) yielding over the net tension area in combination with fracture over the net shear area. It should be noted that the second failure mode considered by AIJ is quite rare and has not been observed in any coped beam test. For the case of double bolt-line connections, which is the focus of the current study, AISC-LRFD and CSA-S16-09 have considered the influence of bolt line on the utilisation level of the tension area, and thus a lower utilisation factor is introduced which is different from that used for single bolt-line connections. On the other hand, the block shear capacity of single and double bolt-line connections are treated using the same equation for either Eurocode 3 or AIJ. In addition, based on a comprehensive numerical study, Topkaya [8] recommended a consistent equation for design of coped beams against block shear failure for both single bolt-line and double bolt-line connections. The design model considered a critical tension plane yield criterion, as shown in Table 5.

### 5.2. Comparisons against existing design rules

Through comparing the test results of 15 specimens (which failed by block shear) against the design equations discussed above, the average test-to-predicted ratios and the associated CoVs (coefficients of variations) are given in Table 4. The remaining two specimens, which failed by local web buckling, were not

**Table 5**
Design equations for block shear in major standards.

| Standards | Design models |
|---|---|
| *AISC-LRFD* | $P_r = \phi(U_{bs}F_uA_{nt} + 0.6F_uA_{nv}) \le \phi(U_{bs}F_uA_{nt} + 0.6F_yA_{gv})$ where $\phi$ = resistance factor, $U_{bs}$ = 1.0 for single bolt line or welded connections; $U_{bs}$ = 0.5 for double or multiple bolt lines, $F_u$ = tensile strength, $F_y$ = yield strength, $A_{nt}$ = net tension area, $A_{nv}$ = net shear area, $A_{gv}$ = gross shear area |
| *Canadian Standard CSA-S16-09* | $P_r = \phi_u\left[U_tF_uA_{nt} + 0.6A_{gv}(F_y + F_u)/2\right]$ where $\phi_u$ = the resistance factor; and $U_t$ = the efficiency factor: $U_t$ = 0.9 for coped beams with single bolt line; $U_t$ = 0.3 for coped beams with double bolt lines |
| *Eurocode 3 EN1993-1-8* | $P_r = 0.5F_uA_{nt}/\gamma_{M2} + (1/\sqrt{3})F_yA_{nv}/\gamma_{M0}$ where $\gamma_{M0}$ = the partial safety factor for resistance of cross-section; $\gamma_{M2}$ = the partial safety factor for resistance of cross-section in tension to fracture |
| *AIJ* | $P_r = \phi[F_uA_{nt} + (1/\sqrt{3})F_yA_{nv}]$ or $P_r = \phi[F_yA_{nt} + (1/\sqrt{3})F_uA_{nv}]$ and the lesser governs the design capacity |
| Topkaya [8] | $P_r = F_yA_{nt} + 0.5F_yA_{gv}$ |

included in the comparison. The resistance factors/partial factors of the design equations were excluded when the comparisons were made. The design tensile resistance of the specimens with staggered bolt arrangements were based on the $s_p^2/4g$ rule. It was observed that the two North American standards AISC-LRFD and CSA-S16-09 lead to similar average test-to-predicted ratios (1.45 for both) on the conservative side, and the associated CoVs are 13.5% and 13.6%, respectively. Eurocode 3 gives the most conservative predictions with an average test-to-predicted ratio of 1.66, but the CoV is slightly lower than those of AISC-LRFD and CSA-S16-09. The conservative prediction of Eurocode 3 mainly attribute to its assumption that the shear resistance is contributed by shear yielding on the net shear area only. As can be seen from the test results, shear yielding was normally developed over (or quite near) the gross shear area, and this has also been confirmed by other independent investigations [6,8]. AIJ appears to provide the average test-to-predicted ratio closest to unity (i.e. 1.08) and it also leads to the least variability (CoV = 11.3%). One of the main reasons for its lower average test-to-predicted ratio compared with the other standards is that no utilisation factor is used over the tension area to consider the non-uniform stress distributions. To sum up, the four considered design standards provide inconsistent predictions on the block shear capacity of the specimens. All the standards tend to be conservative in terms of the average test-to-predicted ratio, and the levels of variability are similar with the CoV ranging between 11.3% and 13.6%. For the design model proposed by Topkaya [8], good agreements with the test results are shown. The test-to-predicted ratio is slightly above unity (indicating conservative predictions), and importantly, the CoV is lower than those obtained from the other design models in major standards. This indicates that the Topkaya's model can be suitable for block shear design of coped beams, especially with double bolt-line connections.

Another interesting and important finding is that the test-to-predict ratios seem to depend on the aspect ratio ($b/a$). The test-to-predict ratios of the specimens with high aspect ratios (i.e. relatively larger shear area) are generally lower than those with low aspect ratios. In other words, the predictions of the standards are more conservative for the specimens with low aspect ratios. A possible explanation is that a decreased shear area (i.e. decreased aspect ratio) can result in a more efficient utilisation of the shear area at ultimate load. As can be seen from the test results, the whole block tear-out (WBT) or TF–WBT failure modes only occurred in the specimens with the aspect ratio less than 1.0. The WBT mode found at ultimate load suggested that the fractural resistance over the gross shear area was almost 'used up' for those specimens, but the design equations do not consider a full utilisation of the fractural resistance of the shear area for necessary levels of conservatism. Therefore, increased test-to-predicted ratios (i.e. more conservative design prediction) are observed for the low aspect ratio specimens which are more prone to WBT.

## 6. Reliability analysis and design recommendations

### 6.1. General

Prior to this study, a total of 13 block shear tests on coped beams with double bolt-line connections were available, which were conducted by Yura et al. [2], Ricles and Yura [3], Franchuk et al. [6], and Fang et al. [9]. The basic information of the previously tested specimens is reproduced in Table 4. Considering all test data (including the current and previous data), the average test-to-predicted ratios and the associated CoVs are given in Table 4. It can be seen that although the major standards are generally on the conservative side, as indicated by the average test-to-predicted ratio, the levels of scatter of the test data are quite high with the CoV ranging between 18.0% and 20.7%. It is also worth mentioning that the test-to-predicted ratios of the specimens studied by Yura et al. [2] and Ricles and Yura [3] are generally lower than those investigated in the current study. This may be due to the fact that the aspect ratios (as reproduced in Table 4) of those specimens [2,3] are relatively high, which can cause decreased test-to-predicted ratios, as explained previously in Section 5.2. With a total of 28 tests on coped beams with double bolt-line connections now available, it is beneficial to re-evaluate the reliability of the existing design standards, especially the rationale behind the current resistance factors.

### 6.2. Procedure of determining resistance factor

The consideration of reliability for any design equation is normally reflected by a resistance factor $\phi$, which is applied to the nominal design resistance to achieve a certain level of safety, e.g. $\phi = 0.75$ in AISC-LRFD and CSA-S16-09 for most failure modes involving rupture. Eurocode 3 employs an alternative term, partial factors, to consider the necessary level of design safety. A common equation used to calculate the resistance factor has been proposed by Ravindra and Galambos [23] and Fisher et al. [24], as expressed by:

$$\phi = C\rho_R e^{(-\beta\alpha_R V_R)} \tag{1}$$

where $\beta$ = safety index, where a higher value indicates a stricter failure probability control (a lower probability of failure). Although there is still argument on the selection of appropriate values of safety index $\beta$, commonly accepted values are 3.0 for members with ductile failure modes, such as beams, and between 4.0 and 4.5 for structural components that fail in a relatively brittle manner, such as connections [25,26]. For the case of block shear failure of coped beam connections, $\beta$ = 4.0–4.5 can be an appropriate target safety index; $\alpha_R$ is a separation factor taken as 0.55 as recommended by Fisher et al. [24]. The constant $C$ is a correction factor for $\phi$ when the safety index is other than 3.0, and it considers the interdependence of the resistance factor and the load factors. Based on the procedure proposed by Fisher et al. [24], an approximated equation for $C$ has been given by Franchuk et al. [7], as expressed by:

$$C = 0.0062\beta^2 - 0.131\beta + 1.338 \tag{2}$$

Finally, $\rho_R$ is the bias coefficient for the resistance; and $V_R$ is the associated CoV for the resistance, as expressed below:

$$\rho_R = \rho_G\rho_M\rho_P\rho_A \tag{3}$$

$$V_R = \sqrt{V_G^2 + V_M^2 + V_P^2 + V_A^2} \tag{4}$$

As indicated in Eqs. (3) and (4), four types of parameter are required to obtain $\rho_R$ and $V_R$. These parameters are related to the variations/uncertainties of 'Geometry', 'Material', 'Professional', and 'Analysis', as summarised below:

- *Geometric variation.* The cause of geometric variation is due to the difference between the actual and nominal dimensions of structural components. The geometry factor $\rho_G$ represents the mean measured-to-nominal ratio of the geometric dimensions of structural members. Through an intensive investigation on the North American steel manufactory markets involving varied suppliers, Kennedy and Gad Aly [27] proposed 0.994 for the geometry factor $\rho_G$ and 3.3% for its CoV $V_G$, and these values were used in the current study.
- *Material variation.* Another source of uncertainty can be caused by the difference between the actual and nominal material strengths. The material factor $\rho_M$ is the mean

measured-to-nominal ratio of material strength. For yielding strength, commonly used material factor $\rho_M$ and the CoV $V_M$ are 1.05% and 6.8% respectively [15,25,26,28]. For tensile strength, based on Dexter et al. [29], Schmidt and Bartlett [25,26] recommended 1.130% and 4.4% to be taken as the material factor $\rho_M$ and its CoV $V_M$, respectively. Considering the complexity of block shear failure which involves a combination of yielding and fracture, a conservative combination of $\rho_M$ and $V_M$ (i.e. lower material factor and higher CoV) was used in this study. Therefore, those for material yielding strength ($\rho_M$ = 1.05% and $V_M$ = 6.8%) were selected.

- *Professional variation.* This represents the variations caused by the difference between the test capacity and that predicted by design equations using measured dimensions and material properties and excluding the resistance factor. The professional factor $\rho_P$ is the mean test-to-predicted ratio of member capacity from available test data, e.g. the test-to-predicted ratios listed in Table 4. Similarly, $V_P$ is the CoV of the test-to-predicted ratios which are also given in Table 4.
- *Analysis variation.* This is used to consider the variations caused by the use of analysis methods other than physical tests, e.g. finite element analysis. As all the data are based on test results, the analysis factor $\rho_A$ and the CoV $V_A$ should be taken as 1.00 and 0.00, respectively.

### 6.3. Analysis results and design recommendations

Employing the above procedure, the required resistance factor $\phi$ for any desirable safety index $\beta$ can be obtained. As the collected data for the variations of geometry and material were based on the North American steel construction market, AISC-LRFD and CSA-S16-09 were selected in this study for reliability analysis. For these two standards, one of the mostly discussed issues is the determination of the utilisation factor of the tension area $U_{bs}$ or $U_t$ to consider the effects of non-uniform stress distribution [28]. For coped beams with double bolt-line connections, $U_{bs}$ = 0.5 and $U_t$ = 0.3 are currently specified in AISC-LRFD and CSA-S16-09, respectively. Alternative values of the utilisation factor were also considered in the reliability analysis. Moreover, two values of safety index, $\beta$ = 4.0 and $\beta$ = 4.5, were considered, which allows the designers to assess the resulting resistance factors under both cases via their own judgements. The obtained resistance factors under the different cases of utilisation factor and safety index are summarised in Table 6.

It can be seen that when $\beta$ = 4.5 needs to be achieved, the resistance factors for the current forms of AISC-LRFD and CSA-S16-09 design equations should be 0.718 and 0.693, respectively. In order for $\phi$ = 0.75 to be consistently used, the utilisation factor for the equation of AISC-LRFD could be adjusted to $U_{bs}$ = 0.4, while for CSA-S16-09, $U_t$ should be less than 0.2. When the safety index is relaxed to $\beta$ = 4.0, the required resistance factors for the current forms of AISC-LRFD and CSA-S16-09 could be relaxed to 0.795 and 0.769, respectively, and in this case $\phi$ = 0.75 is adequately safe for both standards. From an optimization point of view, either the resistance factor $\phi$ or the utilisation factor $U_{bs}/U_t$ can be adjusted in order to achieve a desirable level of safety $\beta$. However, the latter method is preferred because in such way a consistent resistance factor (e.g. $\phi$ = 0.75) can be used throughout the relevant parts of the standards. Therefore, it is recommended that, for $\beta$ = 4.5 to be achieved, $U_{bs}$ = 0.4 and $U_t$ = 0.17 are used for AISC-LRFD and CSA-S16-09, respectively; and for $\beta$ = 4.0, $U_{bs}$ = 0.6 and $U_t$ = 0.33 can be employed. Using these proposed utilisation factors, $\phi$ = 0.75 can be consistently maintained in a safe yet economical manner.

**Table 6**
Reliability analysis results.

| Standards | Parameters | $U_{bs}$ or $U_t$ | | |
|---|---|---|---|---|
| | | 0.4 | 0.5 | 0.6 |
| AISC-LRFD | $\rho_G/V_G$ | 0.994/3.3% | | |
| | $\rho_M/V_M$ | 1.05/6.8% | | |
| | $\rho_P/V_P$ | 1.45/21.0% | 1.33/19.8% | 1.23/18.9% |
| | $\rho_A/V_A$ | 1.00/0.0% | | |
| | $\phi$ ($\beta$ = 4.0) | 0.846 | 0.795 | 0.749 |
| | $\phi$ ($\beta$ = 4.5) | 0.761 | 0.718 | 0.678 |
| | | 0.2 | 0.3 | 0.4 |
| CSA-S16-09 | $\rho_G/V_G$ | 0.994/3.3% | | |
| | $\rho_M/V_M$ | 1.05/6.8% | | |
| | $\rho_P/V_P$ | 1.43/22.0% | 1.31/20.7% | 1.21/19.7% |
| | $\rho_A/V_A$ | 1.00/0.0% | | |
| | $\phi$ ($\beta$ = 4.0) | 0.817 | 0.769 | 0.725 |
| | $\phi$ ($\beta$ = 4.5) | 0.734 | 0.693 | 0.655 |

## 7. Summary and conclusions

This paper has reported a comprehensive investigation on the behaviour and design of block shear failure of coped beams with double bolt-line connections. A total of 17 full-scale tests have been conducted, and the test parameters included web block aspect ratio, out-of-plane eccentricity, connection rotational stiffness, and bolt stagger. Two specimens were found to fail by local web buckling, and the remaining 15 specimens failed by block shear. Three typical block shear failure modes were observed at ultimate load, namely, whole block tear-out (WBT), tensile fracture (TF), and tensile fracture followed by whole block tear-out (TF–WBT). The failure mode was found to be affected by the aspect ratio and connection type. In addition, web twisting was observed in some specimens, and the significance of web twisting was influenced by the lateral stiffness of the connections.

For the block shear capacity, it was found that increasing the shear area could lead to marginal increase of the ultimate reaction. Increasing the tension area could also increase the block shear capacity, where increasing the length of $e_h$ was more effective than increasing the length of $g$. The connection stiffness was also an important factor affecting the block shear capacity. The presence of out-of-plane eccentricity might have detrimental effect on the block shear capacity for the case of double bolt-line connections, but the influence was found to be limited. The detrimental effect might also be associated with the change of connection stiffness for different connection types, and therefore it was difficult to conclude that the decreased block shear capacity was exclusively due to the influence of out-of-plane eccentricity. Therefore, future parametric studies were recommended. Furthermore, staggered bolt arrangements were also found to affect the block shear capacity, but the influence was minor. It was preliminarily suggested that the $s_p^2/4g$ rule could be safely used to obtain the effective tension area along the zigzag bolt pattern, and no change needs to be made for the way treating the shear area.

The test results obtained from the current experimental programme were compared with the existing design rules, where American Standard AISC-LRFD, Canadian Standard CSA-S16-09, Eurocode 3, and Japanese standard AIJ were considered. Inconsistent predictions provided by these standards were generally observed, and the average test-to-predicted ratios for all the four standards were above unity (indicating conservative design models) with the level of CoV ranging between 11.3% and 13.6%. Using the test data obtained from this study, and considering 13 more block shear tests conducted earlier by other researchers, further comparisons against the design equations were performed. The newly obtained average test-to-predicted ratios (considering a total of 28 available tests) confirmed that the major standards are generally on the conservative side for double bolt-line

connections, but the levels of variation are quite high with the CoV ranging from 18.0% to 20.7%. A subsequent reliability analysis was performed on the North American standards AISC-LRFD and CSA-S16-09, and it was found that the specified value of $\phi = 0.7$ 5 might be unsafe for both standards if a safety index of 4.5 was targeted. In order to consistently use the resistance factor $\phi = 0.75$, recommended design equations with newly proposed utilisation factors $U_{bs}/U_t$ were finally given in this paper to cater for different levels of safety index.

## Acknowledgements

The work presented in this paper is substantially supported by the Grant MYRG143(Y1-L2)-FST11-LCC provided by the Research Committee of University of Macau. Partial funding support was also provided by a Grant from The Hong Polytechnic University, Central Research Grant (Project No. G-YBCF). The assistance of the technical staff in the Structural Laboratory of the University of Macau and N.Y. He is also acknowledged.

## References

[1] Birkemoe PC, Gilmor MI. Behavior of bearing critical double-angle beam connections. Eng J 1978;15(4):109–15.
[2] Yura JA, Birkemoe PC, Ricles JM. Beam web shear connections: an experimental study. J Struct Div 1982;108(ST2):311–25.
[3] Ricles JM, Yura JA. Strength of double-row bolted-web connections. J Struct Eng 1983;109(ST12):126–42.
[4] Kulak GL, Grondin GY. AISC LRFD rules for block shear—a review. Eng J 2001;38(4):199–203.
[5] Aalberg A, Larsen PK. Strength and ductility of bolted connections in normal and high strength steels. In: Proceedings of the seventh international symposium on structural failure and plasticity; 2000.
[6] Franchuk CR, Driver RG, Grondin GY. Experimental investigation of block shear failure in coped steel beams. Can J Civ Eng 2003;30(5):871–81.
[7] Franchuk CR, Driver RG, Grondin GY. Reliability analysis of block shear capacity of coped steel beams. J Struct Eng 2004;130(12):1904–13.
[8] Topkaya C. Finite element modeling of block shear failure in coped steel beams. J Constr Steel Res 2007;63(4):544–53.
[9] Fang C, Lam ACC, Yam MCH, Seak KS. Block shear strength of coped beams with single-sided bolted connection. J Constr Steel Res 2013;86:153–66.
[10] Yam MCH, Fang C, Lam ACC, Cheng JJR. Local failures of coped steel beams – a state-of-the-art review. J Constr Steel Res 2014;102:217–32.
[11] Steel Construction Institute. Steelwork design guide to BS5950: Part 1:1990. Volume 1: Section properties, member capacities. 4th ed.; 1997.
[12] American Society for Testing and Materials (ASTM). Standard test methods and definitions for mechanical testing of steel products, ASTM Standard A370-02, Philadelphia, PA; 2002.
[13] Cheng JJR, Yura JA. Local web buckling of coped beams. J Struct Eng 1986;112(10):2314–31.
[14] Yam MCH, Lam ACC, Iu VP, Cheng JJR. The local web buckling strength of coped steel I-beam. J Struct Eng 2003;129(1):3–11.
[15] Yam MCH, Grondin GY, Wei F, Chung KF. Design for block shear of coped beams with a welded end connection. J Struct Eng 2011;137(8):811–21.
[16] ABAQUS Analysis User's Manual. ABAQUS Standard, Version 6.10; 2011.
[17] Cochrane VH. Rules for rivet hole deductions in tension members. Eng News-Record 1922;89:847–8.
[18] Epstein HI, Chamarajanagar R. Finite element studies for correlation with block shear tests. Comput Struct 1996;61(5):967–74.
[19] AISC-LRFD 2010. Load and resistance factor design specification for structural steel buildings. Chicago, IL, USA: American Institute of Steel Construction; 2010.
[20] Canadian Standards Association (CSA). CAN/CSA-S16-09 Limit states design of steel structures. Toronto (ON, Canada); 2009.
[21] EN 1993-1-8:2005. Eurocode 3: design of steel structures – Part 1–8: design of joints. Brussels, Belgium: European Committee for Standardization; 2005.
[22] Architectural Institute of Japan (AIJ). Standard for limit state design of steel structures; 1990.
[23] Ravindra MK, Galambos TV. Load and resistance factor design for steel. J Struct Div 1978;104(9):1337–53.
[24] Fisher JW, Galambos TV, Kulak GL, Ravindra MK. Load and resistance factor design criteria for connectors. J Struct Div 1978;104(9):1427–41.
[25] Schmidt BJ, Bartlett FM. Review of resistance factor for steel: data collection. Can J Civ Eng 2002;29:98–108.
[26] Schmidt BJ, Bartlett FM. Review of resistance factor for steel: resistance distributions and resistance factor calibration. Can J Civ Eng 2002;29:109–18.
[27] Kennedy DJL, Gad Aly M. Limit states design of steel structures – performance factors. Can J Civ Eng 1980;7:45–77.
[28] Oosterhof SA, Driver RG. Performance of the unified block shear equation for common types of welded steel connections. Eng J 2011:77–92. Second Quarter.
[29] Dexter RJ, Graeser M, Saari WK, Pascoe C, Gardner CA, Galambos TV. Structural shape material property survey. Technical Report for Structural Shape Producers Council, University of Minnesota, Minneapolis; 2000.